Modern Control of Induction Machines

Krogsgaard, Mads; Bech, Michael Møller; Andersen, Torben O.

Published in:
Proc. of Nordic Workshop on Power and Industrial Electronics

Publication date:
2006

Document Version
Publisher's PDF, also known as Version of record

Modern Control of Induction Machines

Mads Krogsgaard, Michael M. Bech, and Torben O. Andersen.

***Abstract*— An investigation of current state of the art in rotor field oriented control of induction machines is conducted. Different kinds of flux observers are analyzed with respect to parameter sensitivity and general performance. The evaluation is done by use of modern control theory and by testing in both a simulation model and in experiments.**

The potential of using different kinds of modern control strategies, like adaptive or sliding mode flux observers, are evaluated. The modern algorithms are all compared to standard methods.

***Index Terms*—Induction Machine, Field Oriented Control, Modern Control Strategies, Flux Observer, Parameter Variation.**

I. Introduction

The squirrel cage induction machine (IM) is very often the machine of choice in industrial applications due to its mechanically simple construction and low maintenance requirements. The IM is however relatively difficult to control compared to other types of electrical machines. For high performance control, field oriented control (FOC) is the most widely used control strategy. This strategy requires information of the flux in the machine. Voltage and current model observers are normally used to obtain this information.

These observers require knowledge of the machine's electrical parameters and variations in these parameters lead to incorrect flux estimation and thereby degraded machine performance [4]. The electrical parameters are often not accurately known and they may vary during machine operation due to rise in temperature or change of magnetizing level. Therefore it is desirable to design a flux observer that is less sensitive to parameter variations than the currently used observers.

These areas of research have been shown a great deal of interest in recent years and many scientific papers concerning these subjects are available, e.g. [5], [6], [7], and [8], many of which include the use of different modern control methods, such as online parameter estimation and sliding mode control.

The objective of this paper is to analyze and evaluate two selected flux observers from this group of alternative flux observers. This is [5] and [8] because these represent both an adaptive algorithm and a robust control structure.

The analysis is done by use of modern control theory and by extensive testing. The testing is done with a Matlab/Simulink model and one of the flux observers is also implemented on a digitally controlled induction machine drive system for experimental tests. The drive system is connected to a servo loading system which is used to emulate different load situations.

All simulations and experiments were conducted on an induction motor with the data given in Appendix A.

The authors are with the Institute of Energy Technology, Aalborg University, Denmark. Phone: (+45) 9635 9278, email: {mkr, mmb, toa}@iet.aau.dk.

II. General rotor field oriented control scheme

A. Model of Induction Machine

It is well known that the IM can be described by the following complex space vector equations in an arbitrary rotating reference frame *K* [2]

$$\overline{u}_{sK} = R_s \cdot \overline{i}_{sK} + \frac{d\overline{\psi}_{sK}}{dt} + j \cdot \omega_K \cdot \overline{\psi}_{sK} \quad (1)$$

$$\overline{0} = R_r \cdot \overline{i}_{rK} + \frac{d\overline{\psi}_{rK}}{dt} + j \cdot \left(\omega_K - p_b \cdot \omega_m\right) \cdot \overline{\psi}_{rK} \quad (2)$$

$$\overline{\psi}_{sK} = L_s \cdot \overline{i}_{sK} + L_m \cdot \overline{i}_{rK} \quad (3)$$

$$\overline{\psi}_{rK} = L_m \cdot \overline{i}_{sK} + L_r \cdot \overline{i}_{rK} \quad (4)$$

$$T_e = \frac{3}{2} \cdot p_b \cdot \frac{L_m}{L_r} \cdot \mathrm{Im}\left(\overline{\psi}^*_{rK} \cdot \overline{i}_{sK}\right). \quad (5)$$

In the above equations, subscript "s" denotes stator and "r" denotes rotor. "p_b" is the pole pair and "j" is the imaginary unit. ω_K is the angular velocity of the reference frame.

The stationary reference frame $\left(\omega_K = 0\right)$ is denoted "$\alpha\beta$" and the frame rotating with the rotor flux is denoted "dq".

B. Basic Methods for Flux Estimation

To conduct proper rotor field oriented control it is necessary to estimate the rotor flux angle, θ_{rf}, since it is not possible to measure the magnetic orientation of the rotor flux.

The two commonly used structures are IFOC and DFOC (indirect and direct rotor FOC). They both have the drawback that they are quite sensitive to variation of the electrical parameters. This results in deteriorated performance, see chapter 8 in [3].

If a standard IFOC structure is used in the controller, it is very important to have an exact knowledge about the value of the rotor time constant, T_r, because it is used in the feed forward slip estimation, see Eq. (6) and (7).

$$\hat{\theta}_{rf} = \int p_b \cdot \omega_m \, dt + \int \frac{1}{\hat{T}_r} \cdot \frac{i_q}{i_d} dt \tag{6}$$

$$\hat{T}_r = \frac{\hat{L}_r}{\hat{R}_r} \tag{7}$$

The "^"-operator denotes estimated values. The main problem is that both parameters in Eq. (7) may vary during operation. In [1] it is found that the rotor resistance because of heating may differ up to around 30% from its rated value. Also it is found that the magnetizing inductance, L_m, may vary in the interval [0.85, 1.32] · $L_{m,rated}$ (for the given motor) due to changes in the magnetizing level.

For DFOC, two basic models - the voltage and current model (VM and CM) – exist [4]. The CM is given in Eq. (8) and the VM in Eq. (9).

Current model in stationary coordinates:

$$p\hat{\overline{\psi}}_{r,CM} = \frac{\hat{R}_r \cdot \hat{L}_m}{\hat{L}_r} \cdot \overline{I}_s - \hat{\omega}_{br} \cdot \hat{\overline{\psi}}_r \tag{8}$$

where $\hat{\omega}_{br} = \frac{\hat{R}_r}{\hat{L}_r} - j \cdot p_b \cdot \omega_m$ and p denotes the differential operator.

Voltage model in stationary coordinates:

$$\left\{ \begin{array}{l} p\hat{\overline{\psi}}_s = \overline{U}_s - \hat{R}_s \cdot \overline{i}_s \\ \hat{\overline{\psi}}_{r,VM} = \frac{\hat{L}_r}{\hat{L}_m} \cdot \hat{\overline{\psi}}_s - \frac{\hat{\sigma}}{1-\hat{\sigma}} \cdot \hat{L}_m \cdot \overline{i} \end{array} \right\} \tag{9}$$

where $\hat{\sigma} = 1 - \frac{\hat{L}_m^{\,2}}{\hat{L}_r \cdot \hat{L}_s}$

It is possible to combine the CM and VM into what is known as a Gopinath observer [4]. This observer reduces the effects of parameter variations by combining the advantages of the CM at low slip velocity and the advantages of the VM at high speed. This observer structure is shown in Fig. 1.

In [4] plots are shown that demonstrates that the Gopinath observer is significantly less affected by parameter errors compared to the VM and CM respectively.

III. ADVANCED FLUX OBSERVERS

Several different modern flux observers were analyzed and evaluated in the project [1], among others [5], [6], [7] and [8]. The principle of the proposed observers in [5] and [6] is a method for adaptation of the rotor time constant, T_r.

A. Adaptive Estimation of T_r Based on Flux Error

In [5] a MRAC (Model Reference Adaptive Control) estimation of the rotor time constant is conducted. The VM is used as a reference model and the CM is used as the plant.

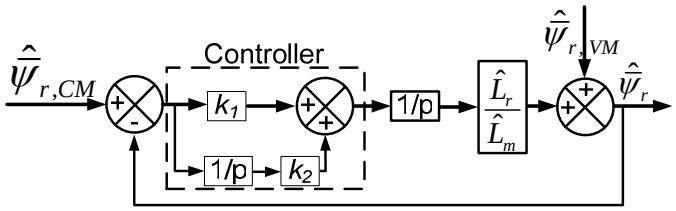

Fig. 1. Gopinath style flux observer. The current model is dominant at low speed and the voltage model is dominant at high speed.

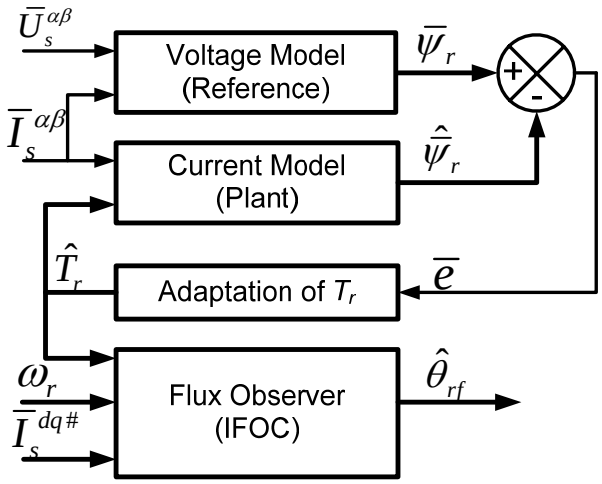

Fig. 2. Block diagram for the MRAC estimation of T_r used in [4]. $\overline{e}$ is an error signal.

In other words (8) and (9) are both implemented and the difference between them is used as an error signal, by which T_r is adjusted.

The adaptation formula used in [5] is given by (10).

$$\frac{1}{\hat{T}_r} = \Phi_1 + \int_0^{t_1} \Phi_2 d\tau \tag{10}$$

$$\Phi_1 = K_1 \cdot \left(e_{r\alpha} \cdot \left(L_m \cdot i_{s\alpha} - \hat{\psi}_{r\alpha} \right) + e_{r\beta} \cdot \left(L_m \cdot i_{s\beta} - \hat{\psi}_{r\beta} \right) \right)$$

$$\Phi_2 = \frac{K_2}{K_1} \cdot \Phi_1, \qquad K_1, K_2 > 0$$

Stability

The globally asymptotically stability of the observer structure is now proved by use of the Popov hyperstability criteria [9].

The error is given as the difference between the actual rotorflux (from the VM) and estimated one (from the CM), see (11).

$$\begin{bmatrix} e_{r\alpha} \\ e_{r\beta} \end{bmatrix} = \begin{bmatrix} \psi_{r\alpha} - \hat{\psi}_{r\alpha} \\ \psi_{r\beta} - \hat{\psi}_{r\beta} \end{bmatrix} \tag{11}$$

The error dynamic is the derivative of (11), and by mathematical manipulations of (1)-(4) and (8)-(9), it is possible to shown that the error dynamic is given by (12), when $\hat{T}_r = T_r$ and $\hat{L}_m = L_m$ [1].

$$\begin{bmatrix} \dot{e}_{r\alpha} \\ \dot{e}_{r\beta} \end{bmatrix} = \begin{bmatrix} -\frac{1}{T_r} & -\omega_e \\ \omega_e & -\frac{1}{T_r} \end{bmatrix} \cdot \begin{bmatrix} e_{r\alpha} \\ e_{r\beta} \end{bmatrix} \tag{12}$$

It is easily seen that the matrix in (12) is Hurwitz, and therefore it can be concluded that the error will approach zero exponentially, if the estimated motor parameters are correct.

However, that is not necessarily the case, and therefore the following expression for the difference between $\hat{T}_r$ and T_r is given, see (13).

$$\frac{1}{\hat{T}_r} = \frac{1}{T_r} - \Delta\frac{1}{T_r} \tag{13}$$

When this expression is used to calculate the error dynamic, it will be given by (14).

$$\begin{bmatrix} \dot{e}_{r\alpha} \\ \dot{e}_{r\beta} \end{bmatrix} = \begin{bmatrix} -\frac{1}{T_r} & -\omega_e \\ \omega_e & -\frac{1}{T_r} \end{bmatrix} \cdot \begin{bmatrix} e_{r\alpha} \\ e_{r\beta} \end{bmatrix} - \left(\frac{1}{T_r} - \frac{1}{\hat{T}_r}\right) \cdot \begin{bmatrix} \hat{\psi}_{r\alpha} - L_m \cdot i_{s\alpha} \\ \hat{\psi}_{r\beta} - L_m \cdot i_{s\beta} \end{bmatrix}$$

$$\Downarrow$$

$$\dot{\bar{e}}_r = \bar{\bar{A}} \cdot \bar{e}_r - \bar{W} \tag{14}$$

From the second part of the right side in (14) it is obvious that the error will not approach zero if the estimated rotor time constant varies from the actual one.

The main problem in adaptive control is indeed to design a control law that ensures the error approaches zero and the system remains stable under parameter variation.

The Popov hyper stability-criteria apply for systems on the form of Fig. 3.A.

From Fig. 3.A it is seen that the system is a combination of a linear time-independent block and a non-linear time-varying feedback-term. This is indeed the shape of (14), and therefore Popovs criteria can be applied for the given system.

The hyperstability-criteria requires that (15) is satisfied:

$$\int_0^{t_1} \bar{e}_r^T \cdot \bar{W} \cdot dt \geq -\gamma^2 \quad \forall t_1 \geq 0 \quad \text{where} \quad \gamma^2 > 0 \tag{15}$$

The proposed adaptation law (10) is now used to prove that (15) is indeed satisfied for the given system.

This gives the following equation:

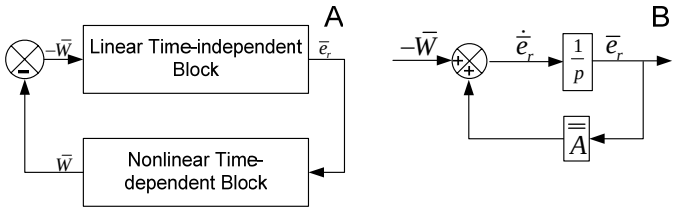

Fig. 3. Popov's hyperstability-criteria is used for systems, which can be brought on the form of A. On part B, the content of the LTI block is shown.

$$\int_0^{t_1} \left[\bar{e}_r^T \cdot \left(\frac{1}{T_r} - \Phi_1 - \int_0^{t_1} \Phi_2 d\tau \right) \begin{bmatrix} \hat{\psi}_{r\alpha} - L_m \cdot i_{s\alpha} \\ \hat{\psi}_{r\beta} - L_m \cdot i_{s\beta} \end{bmatrix} \right] dt \geq -\gamma^2 \tag{16}$$

For simplicity, let

$$\begin{aligned} \tilde{\psi}_{r\alpha} &= \hat{\psi}_{r\alpha} - L_m \cdot i_{s\alpha} \\ \tilde{\psi}_{r\beta} &= \hat{\psi}_{r\beta} - L_m \cdot i_{s\beta}. \end{aligned} \tag{17}$$

Also note that inserting (17) into (10) results in:

$$\begin{aligned} \Phi_1 &= -K_1 \cdot \left(e_{r\alpha} \cdot \tilde{\psi}_{r\alpha} + e_{r\beta} \cdot \tilde{\psi}_{r\beta} \right) \\ \Phi_2 &= -K_2 \cdot \left(e_{r\alpha} \cdot \tilde{\psi}_{r\alpha} + e_{r\beta} \cdot \tilde{\psi}_{r\beta} \right). \end{aligned} \tag{18}$$

Substituting (17) and (18) into (16) yields

$$\int_0^{t_1} \left[\left(e_{r\alpha}\tilde{\psi}_{r\alpha} + e_{r\beta}\tilde{\psi}_{r\beta} \right) \cdot \left(\frac{1}{T_r} - \Phi_1 - \int_0^{t_1} \Phi_2 d\tau \right) \right] dt \geq -\gamma^2$$

$$\Updownarrow$$

$$\int_0^{t_1} \left[\left(e_{r\alpha}\tilde{\psi}_{r\alpha} + e_{r\beta}\tilde{\psi}_{r\beta} \right) \left(\frac{1}{T_r} + K_1 \left(e_{r\alpha}\tilde{\psi}_{r\alpha} + e_{r\beta}\tilde{\psi}_{r\beta} \right) + \int_0^{t_1} K_2 \left(e_{r\alpha}\tilde{\psi}_{r\alpha} + e_{r\beta}\tilde{\psi}_{r\beta} \right) d\tau \right) \right] dt \geq -\gamma^2. \tag{19}$$

Now, let:

$$\begin{aligned} f(t) &= \frac{1}{T_r} + \int_0^{t_1} K_2 \left(e_{r\alpha}\tilde{\psi}_{r\alpha} + e_{r\beta}\tilde{\psi}_{r\beta} \right) d\tau \\ \dot{f}(t) &= \frac{df}{dt} = K_2 \left(e_{r\alpha}\tilde{\psi}_{r\alpha} + e_{r\beta}\tilde{\psi}_{r\beta} \right) \end{aligned} \tag{20}$$

Equation (20) is now substituted into (19) to find the lower boundary on the integral.

$$\int_0^{t_1} \left[\frac{1}{K_2} \cdot \dot{f}(t) \cdot \left(\frac{K_1}{K_2} \cdot \dot{f}(t) + f(t) \right) \right] dt \geq -\gamma^2$$

$$\Updownarrow$$

$$\frac{K_1}{K_2^2}\cdot\int_0^{t_1}\dot{f}^2(t)\,dt+\frac{1}{K_2}\cdot\int_0^{t_1}\dot{f}(t)\cdot f(t)\,dt\geq-\gamma^2$$

$$\Updownarrow$$

$$\frac{K_1}{K_2^2}\cdot\int_0^{t_1}\dot{f}^2(t)\,dt+\frac{1}{K_2}\cdot\int_{f(0)}^{f(t_1)}f\cdot df\geq-\gamma^2 \qquad (21)$$

Now the stability proof is reduced to show that (21) is true, which is rather easy.

The lower boundaries on the integrals are found to be:

$$\left.\begin{aligned}&\frac{K_1}{K_2^2}\cdot\int_0^{t_1}\dot{f}^2(t)\,dt\geq 0\\&\frac{1}{K_2}\cdot\int_{f(0)}^{f(t_1)}f\cdot df=\frac{1}{2K_2}\left(f^2(t_1)-f^2(0)\right)\\&\qquad\geq-\frac{f^2(0)}{2\cdot K_2}=-\frac{1}{2\cdot K_2\cdot T_r^2}\end{aligned}\right\}\Rightarrow$$

$$\frac{K_1}{K_2^2}\cdot\int_0^{t_1}\dot{f}^2(t)\,dt+\frac{1}{K_2}\cdot\int_{f(0)}^{f(t_1)}f\cdot df\geq-\frac{1}{2\cdot K_2\cdot T_r^2}$$

$$\Updownarrow$$

$$\int_0^{t_1}\overline{e}_r^{\,T}\cdot\overline{W}\cdot dt\geq-\frac{1}{2\cdot K_2\cdot T_r^2}=-\gamma^2 \qquad (22)$$

Hereby it is proved that (15) indeed is true, since a value, $-\gamma^2$, exists, which the integral always is larger than or equal to. This was exactly the required condition for stability.

Simulations

Simulations of the observer structure demonstrated that – given a correct reference model – the adaptation mechanism was able to find the correct value of $\hat{T}_r$ if $\hat{R}_{r,initial}$ and/or $\hat{L}_{m,initial}$ was set different from the values used in the simulation of the induction motor. Fig. 4.A shows a simulation with an error on the rotor resistance – it is initially set 30% above its rated value (simulating a heating of the rotor). Thereby the actual rotor time constant is about 77% of its rated value. It is seen that the correct value of the rotor time constant is estimated in about 0.6 s.

However, it was also found that if the stator resistance used in the controller, $\hat{R}_s$ was set different from R_s, the control algorithm was not able to estimate the correct rotor time constant, in fact it began to oscillate heavily, see Fig. 4.B. No steady state point was reached and $\hat{T}_r$ kept fluctuating within the shaded area, so it was necessary to filter the value to get an average value (filtered version also shown on part B).

This would be the case in real life, because due to heating the stator and rotor resistance will not vary independently.

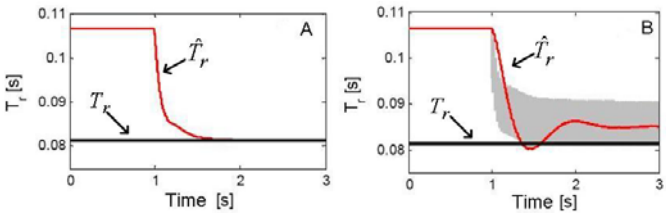

Fig. 4. Simulations, where the value of R_r is set 30% above its rated value. The adaptation algorithm was switched on at time=1 s. Part A shows the adaptation, when $R_s = R_{s,rated}$. Part B shows the adaptation, when $R_s = 1.3\cdot R_{s,rated}$.

Based on these simulations it can be concluded that the algorithm only will work with a correct reference model, e.g. the voltage model (9) will provide a correct flux estimate. But if that was the case, then it would be better just to use the VM as the flux observer, since it then also would be possible to conduct a closed loop control on the flux amplitude, and also the controller would be less complicated.

B. Velocity Independent Sliding Mode Flux Observer

In [8] another kind of flux observer is proposed. This is also based on a comparison between the current and voltage model, but instead of constructing some sort adaptation algorithm a sliding mode contribution is added to both the CM and VM based on a current error.

In [8] the proposed velocity independent sliding mode flux observer (SMO) is used in a VSC-DTC algorithm (Variable-Structure-Control Direct-Torque-Control), and very good results are obtained. Here, the SMO is used in a DFOC strategy, where the rotor flux angle and amplitude is extracted from the model.

It is possible to rewrite the CM and VM to (23 a-c), where the VM is given in the $\alpha\beta$-frame and CM in the rotor-flux oriented frame.

$$\begin{aligned}&p\hat{\overline{\psi}}_s^{\alpha\beta}=-R_s\cdot\overline{i}_s^{\alpha\beta}+\overline{U}_s^{\alpha\beta}+K_1\cdot\overline{\upsilon} && (a)\\&p\hat{\overline{\psi}}_r^{dq}=-\left(\frac{1}{T_r\cdot\sigma}+j\cdot\left(\omega_{rf}-p_b\cdot\omega_m\right)\right)\cdot\hat{\overline{\psi}}_r^{dq}\\&\qquad+\frac{L_m}{L_s\cdot T_r\cdot\sigma}\cdot\hat{\overline{\psi}}_s^{\alpha\beta}\cdot e^{-j\cdot\hat{\theta}_{rf}}+K_2\cdot\overline{\upsilon}\cdot e^{-j\cdot\hat{\theta}_{rf}} && (b)\\&\hat{\overline{I}}_s^{\alpha\beta}=\frac{1}{L_s\cdot L_r\cdot\sigma}\cdot\left(L_r\cdot\hat{\overline{\psi}}_s^{\alpha\beta}-L_m\cdot\hat{\overline{\psi}}_r^{dq}\cdot e^{j\cdot\hat{\theta}_{rf}}\right) && (c)\end{aligned} \qquad (23)$$

Since $\psi_{rq}=0$ in the rotor flux-oriented reference frame it also means that the imaginary part of (23.b) is zero. Thereby the observer is velocity independent, since the term $j\cdot\left(\omega_{rf}-p_b\cdot\omega_m\right)$ vanishes from the equation.

It is also seen that an extra term is added in (23.a) and (23.b). K_1 and K_2 are velocity dependant terms given by (24) [8]:

$$K_1 = k_{1r} + j \cdot k_{1i} \cdot \omega_m^{\#} \quad K_2 = k_{2r} + j \cdot k_{2i} \cdot \omega_m^{\#} \quad (24)$$

(by using the reference velocity, $\omega_m^{\#}$, instead of the actual velocity in Eq. (12), the observer is still sensorless and less noisy).

According to [8] $\overline{\upsilon}$ is given by (25):

$$\overline{\upsilon} = \overline{e}_{Is} + K_{\text{SMO}} \cdot \left(\text{sgn}\left(e_{isd}\right) + j \cdot \text{sgn}\left(e_{isq}\right) \right)$$
$$\overline{e}_{Is} = e_{isd} + j \cdot e_{isq} = \overline{I}_s^{\alpha\beta} - \hat{\overline{I}}_s^{\alpha\beta} \quad (25)$$

The observer structure is shown on block diagram form in Fig. 6.

This observer structure was tested both in a simulation model and on the experimental setup under various speed and load conditions. The effects of parameter variations were analyzed and the results compared to the Gopinath observer.

In [8] it is mentioned that this observer structure is sensitive to variation of the stator resistance at low speed. This is also seen on the plots in Fig. 7. These plots were made by use of the simulation model, where the estimated flux angle and amplitude were compared to the simulated values.

Fig. 7 shows that the SMO is significant less sensitive to parameter variations except at low speed when loaded, which is a well known problem for sensorless control.

As mentioned before it turned out that the sliding mode observer was unstable at low speed when loaded, which was due to stator resistance variance. This is also brought up in [8] and an R_s-estimation algorithm is proposed. However, in [1] it is found that better results can be expected if only the flux angle is extracted from the observer and no closed loop control on the amplitude of flux is conducted. Even though the flux level is computed in open loop experimental tests showed that this control algorithm will produce good dynamic responses, see Fig. 5.

IV. Conclusion

In this paper two different kinds of advanced flux observers are evaluated. It is found that the adaptive algorithm in [5] is able to estimate the rotor time constant accurately and thereby also provide a correct flux estimate. However this was only the case, when the reference model was correct, i.e. the stator resistance was well known. Otherwise performance will be significantly deteriorated.

The velocity independent sliding mode flux observer proposed in [8] shows promising results, since it demonstrates a higher precision than the classical flux observers, when the knowledge of the electrical parameters is inaccurate. Also both the experimental work in [1] and the results shown in [8] demonstrates that this kind of robust flux observer has a significant potential in practical applications.

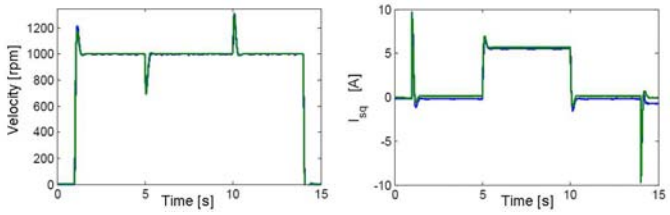

Fig. 5. Comparison of the experimental and simulated results for the SMO. To the left the velocity response is shown when a reference of 1000 rpm is given (after 1 s.). Load steps from 0 Nm to 14.7 Nm and back to 0 Nm is given at 5 and 10 s. respectively. After 14 s. the speed reference is again set to zero. To the right the corresponding q-axis current is shown.

Appendix

A. Motor Data

All simulations and experiments were conducted on an induction motor with the following rated data

$U = 380V$ (Y) $I = 5.0A$ $P = 2.2kW$

$L_{ls} = 9.2mH$ $L_{lr} = 12.29mH$ $L_m = 235mH$

$R_s = 3.67\Omega$ $R_r = 2.32\Omega$ 4 poles

$n_{\text{rated}} = 1430$ rpm $T_{rated} = 14.7Nm.$

A sample frequency of 5000 Hz is used for conducting the digital control on the experimental setup.

References

[1] P. L. Christensen, M. Krogsgaard, and C.N. Thomsen, “Modern Control of Induction Machines”. Masters thesis, Aalborg University, 2005.

[2] M. P. Kazmierkowski and H. Tunia, “Automatic Control of Converter-Fed Drives”. Elsevier 1994.

[3] D.W. Novotny and T.A. Lipo, “Vector Control and Dynamics of AC Drives”. Clarendon Press Oxford 1996.

[4] P.L. Jansen and R.D. Lorenz, “A Physically Insightful Approach to the Design and Accuracy Assessment of Flux Observers for Field Oriented Induction Motor Drives”. Industry Applications, IEEE Transactions on. Volume 30, Issue 1, Jan-Feb. 1994 Page(s) 101-110.

[5] K.-K. Shyu, H.-J. Shieh, and C-C. Liu, “Adaptive Field-Oriented Control of Induction Motor with Rotor Flux Observation. Industrial Electronics, Control and Instrumentation, 1996. Proceedings of the 1996 IEEE IECON 22nd International Conference on. Volume 2, 5-10 Aug. 1996 Page(s): 1204-1209 vol. 2.

[6] S.-B. Cho and D.-S. Hyun, “A Robust Indirect Vector Control for the Rotor Time Constant Variation of Induction Machines. Industrial Electronics, Control and Instrumentation, 1996. 22nd International Conference on Proceedings of the 1996 IEEE IECON. Volume 2, 5-10 Aug. 1996 Page(s): 1240-1245 vol. 2.

[7] H.-U. Rehman, “Elimination of the Stator Resistance Sensitivity and Voltage Sensor Requirement Problems for DFO Control of an Induction Machine”. IEEE Transactions on Industrial Electronics. Volume 52, Issue 1, Feb. 2005 Page(s): 263-269.

[8] C. Lascu, I. Boldea, and F. Blaabjerg, “Very-Low-Speed Variable-Structure Control of Sensorless Induction Machine Drives Without Signal Injection”. Industry Applications, IEEE Transactions on. Volume 41, Issue 2, March-April 2005, Page(s): 591-598.

[9] I. D. Landau, “A Hyperstability Criterion for Model Reference Adaptive Control Systems”, IEEE Transactions on Automatic Control, October 1969 Page(s) 552-555.

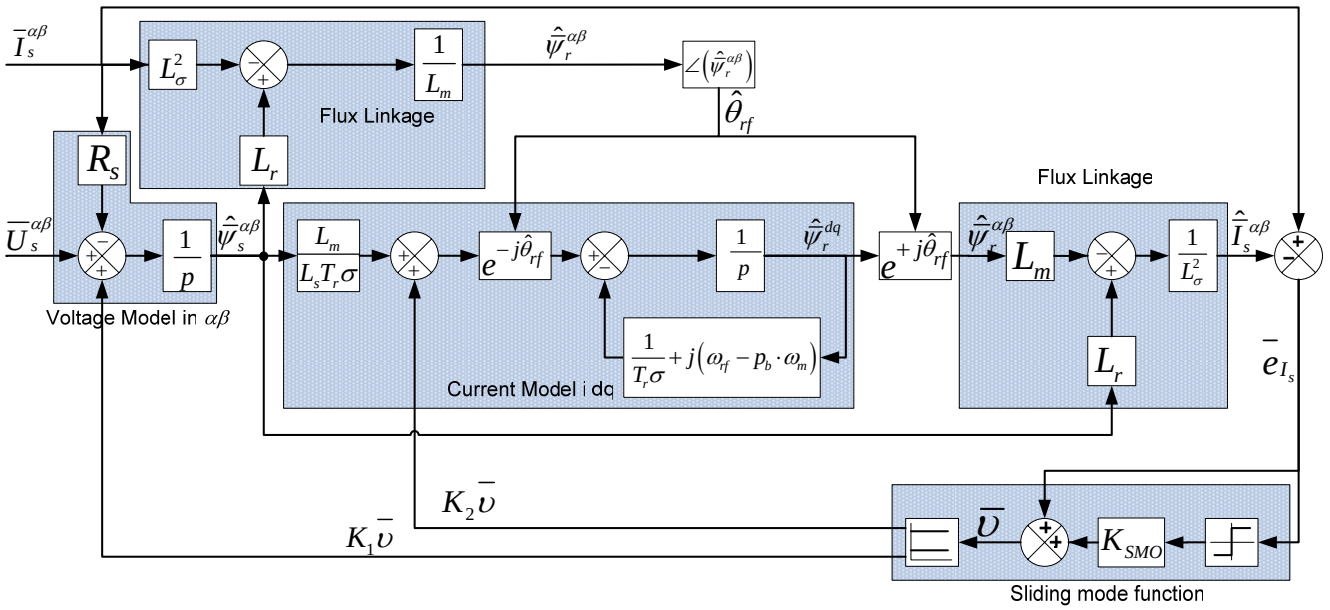

Fig. 6. Block diagram of the velocity independent sliding mode flux observer. A sliding mode function based on a current error is used to correct the voltage and current model.

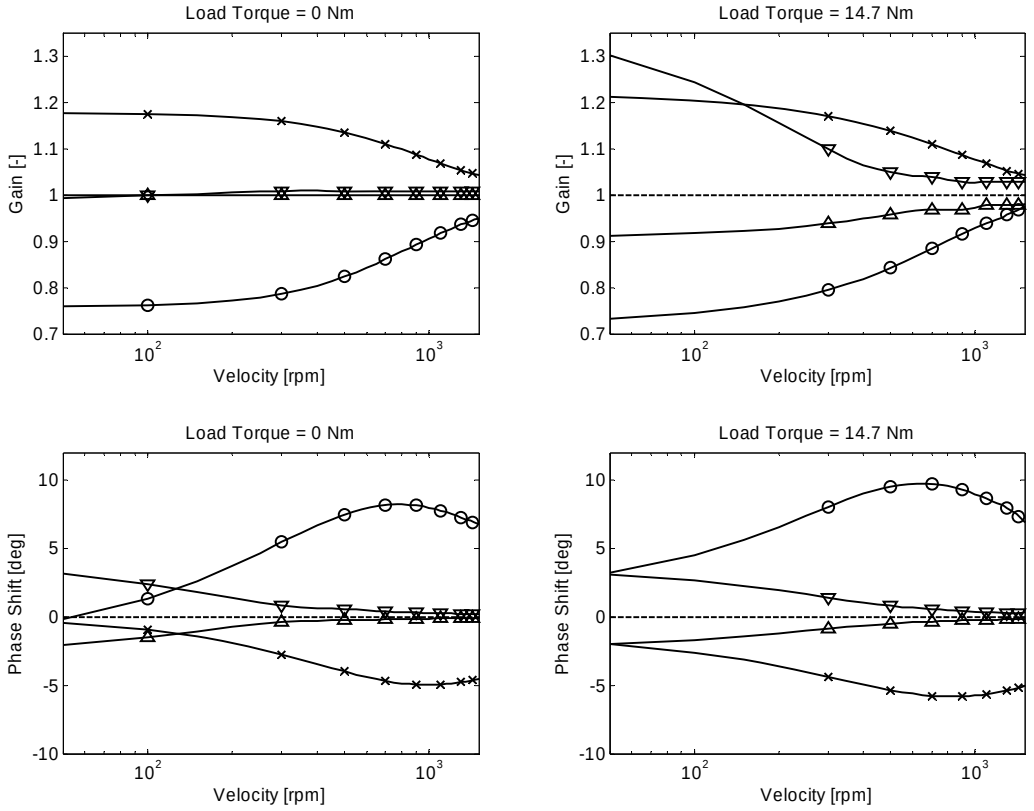

Fig. 7. Parameter sensitivity of the sliding mode observer compared to the Gopinath observer. The two left figures are for the noload situation and the two figures to the right are for rated load (14.7 Nm). The graphs are found from the simulation model.

The "Δ"-marked curve is for the sliding mode observer with parameter estimates: $\hat{R}_s = 0.85 \cdot R_s$, $\hat{R}_r = 0.85 \cdot R_r$, $\hat{L}_m = 0.85 \cdot L_m$ (all minimum)

The "∇"-marked curve is for the sliding mode observer with parameter estimates: $\hat{R}_s = 1.3 \cdot R_s$, $\hat{R}_r = 1.3 \cdot R_r$, $\hat{L}_m = 1.32 \cdot L_m$ (all maximum)

The "O"-marked curve is for the Gopinath observer with parameter estimates: $\hat{R}_s = 0.85 \cdot R_s$, $\hat{R}_r = 0.85 \cdot R_r$, $\hat{L}_m = 0.85 \cdot L_m$ (all minimum)

The "x"-marked curve is for the Gopinath observer with parameter estimates: $\hat{R}_s = 1.3 \cdot R_s$, $\hat{R}_r = 1.3 \cdot R_r$, $\hat{L}_m = 1.32 \cdot L_m$ (all maximum)